運輸省港湾技術研究所

港湾技術研究所報告

REPORT OF THE PORT AND HARBOUR RESEARCH INSTITUTE

MINISTRY OF TRANSPORT

VOL. 8 NO. 1 MAR. 1969

NAGASE, YOKOSUKA, JAPAN

港湾技術研究所報告は第7巻第1号より年4回定期的に刊行する。ただし第1巻から第6巻および欧文編第1号から第15号までは下記のとおり不定期に刊行された。

報告の入手を希望する方は論文番号を明記して港湾技術研究所長に申し込んで下さい。

和 文 篇 (Japanese Edition)

Vol. 1. No. 1 (1963)
Vol. 2. Nos. 1～3 (1963～1964)
Vol. 3. Nos. 1～7 (1964)
Vol. 4. Nos. 1～11 (1965)
Vol. 5. Nos. 1～15 (1966)
Vol. 6. Nos. 1～8 (1967)

欧 文 篇 (English Edition)

Report Nos. 1～15 (1963～1967)

The Report of the Port and Harbour Research Institute is published quarterly, either in Japanese or in occidental languages. The title and synopsis are given both in Japanese and in occidental languages.

The report prior to the seventh volume were published in two series in Japanese and English as listed above.

The copies of the Report are distributed to the agencies interested on the basis of mutual exchange of technical publication.

Inquiries relating to the Report should be addressed to the director of the Institute specifying the numbers of papers in concern.

港湾技術研究所報告 (REPORT OF P.H.R.I.)

第8巻 第1号 (Vol. 8, No. 1), 1969年3月 (March 1969)

目 次 (CONTENTS)

1. Measurement of Wind Velocity Fluctuations over Waves in a Wind-Wave Tunnel ……Hajime KATO and Kikuo SANO…… 3

(風洞水路における波の上の風速変動の性質について……加藤 始・佐野喜久雄)

2. 沖積粘土層におけるサウンディング (数種の方法による試験結果について) …… 柳瀬重靖…… 37

(Soundings in the Alluvial Clay Stratums (On the results of several methods) …… Shigeyasu YANASE)

3. 粕土試料の攪乱に関する研究 (第1報) ——繰り返し三軸圧縮試験による攪乱実験—— ……奥村樹郎…… 59

(Studies on the Disturbance of Clay Samples (1st Report)——Remolding Tests by the Repeated Triaxial Compression—— ……Tatsuro OKUMURA)

4. 飽和砂層の振動性状 ……荒井秀夫・梅原靖文…… 85

(Vibration of Saturated Sand Layears …… Hideo ARAI and Yasuhumi UMEHARA)

5. 音響測深機に関する研究 ……木原純孝……123

(Study on Echo-Sounder……Sumitaka KIHARA)

6. 砂，砂利混合時の浚渫ポンプの特性 …… 八木得次・宮崎昭児・奥出 律……165

(Characteristic of the Dredging Pump in Case of Mixed with Sand and Gravel …… Tokuji YAGI, Shoji MIYAZAKI and Tadasu OKUDE)

REPORT OF THE PORT AND
HARBOUR RESEARCH INSTITUTE
Vol. 8 No. 1 (Mar. 1969)

1. Measurements of Wind Velocity Fluctuations over Waves in a Wind-Wave Tunnel

Hajime KATO*
Kikuo SANO**

Synopsis

A linearized hot-wire anemometer was used to sense the longitudinal velocity fluctuations in wind both over the long periodic waves superposed by much smaller wind waves and over the wind waves only, in a wind-wave tunnel. The wind data were recorded digitally and analysed to obtain wind velocity spectra over a frequency range from 0.1 to 720 c/s by the digital procedures which involve the divided computations to cover the wide frequency range. In order to find out the direct relations between those velocity fluctuations and waves, the cross-spectra between the two were also estimated.

Wind velocity spectra obtained show a range of frequencies where the spectral density varies nearly as $f^{-5/3}$ (f: frequency), and this range is extended to much lower frequencies than expected from Kolmogoroff's theory. Over the wind waves only, the wave-induced velocity fluctuations were found to have a considerable intensity at the lowest height, decrease fairly rapidly with height and become almost negligible at the height of 15 cm. Over the said long waves the wave-induced fluctuations were only moderately strong near the wave crests, the spectrum showing a very small peak at the frequency of the long waves. But they did not decay very much with height and remained at the height of 40 cm as a dominant component of the spectrum. It was found that those wave-induced fluctuations were nearly in phase with the dominant waves and that the phase of the fluctuations was leading that of waves by a small quantity, but with a probable exception near the crests in the case of the long waves.

* Chief, Storm Surge and Tsunami Laboratory, Hydraulics Division.
** Member of Hydraulics Laboratory.

港湾技術研究所報告
第8巻 第1号 (1969. 3)

1. 風洞水路における波の上の風速変動の性質について

加 藤 始*・佐 野 喜 久 雄**

要 旨

熱線風速計を使って，風洞水路において小さな風波に重畳された長周期波および風波だけの場合につき，その上を吹く風の水平速度変動成分を測定した。それらのデータはデイジタルデータレコーダに記録し，0.1 c/s から 720 c/s の広い周波数範囲について分割計算によるデイジタルの方法で，風速変動のスペクトルを求めた。またそれらの風速変動と波との間の直接の関係を見出すために，両者のクロススペクトルも計算した。

求められた風速変動スペクトルは，スペクトル密度が周波数の $-5/3$ 乗で変化する周波数領域を示し，この領域は，Kolmogoroff の理論から予想されるよりももっと低い周波数にまでのびている。風波だけの場合の波によって生じた風速変動は，波のすぐ上では目立った強度をもつが，高さと共にかなり急速に減衰し，15 cm の高さではほとんど無視しうるようになることが見出された。上記の長周期波の場合の波による風速変動は，波のすぐ上ではそれほど強くなく，そこでの風速変動スペクトルは，その長周期波の周波数において非常に小さなピークしか示さない。しかし，その波による風速変動は高さと共にあまり減衰せず，高さ 40 cm ではスペクトルの非常に卓越した成分として残る。これらの波によって生じた風速変動は，卓越した波と大体同位相で，その変動の位相の方が波の位相より多少進んでいるが，長周期波のすぐ上の場合だけは波の位相の方が少し進んでいるらしいことが見出された。

* 水工部 高潮津波研究室長
** 水工部 水理研究室

CONTENTS

Synopsis 3

1. **Introduction** 7

2. **Experimental Equipment and Procedures** 8

2.1 General Description of Experiments 8

2.2 Hot-Wire Anemometer and Other Instruments 9

2.3 Measurements of Wind Velocity Spectra 11

2.4 Measurements of Cross-Spectra between Wind and Waves 13

3. **Results and Discussion** 18

3.1 Data for Mean Wind 18

3.2 Wind Velocity Spectra 19

3.3 Cross-Spectra between Wind and Waves 24

4. **Conclusions** 33

Acknowledgement 34

References 34

1. Introduction

The boundary layer of wind over water is distinctly different from other boundary layers in that the nature of the boundary itself changes with wind and can not be prescribed. The study of the wind boundary layer is closely connected with, or more precisely a part of, that of wave generation by wind.

Since the two wave generation theories were proposed with different mechanisms by O. M. Phillips and J. W. Miles, respectively, in 1957, measurements have often been made of winds over waves as well as the waves both in the laboratories and in the fields in order to check those theories. Lighthill's interpretation[13] together with the accumulating results seemed to be establishing the validity of the inviscid laminar model proposed by Miles (1957). Recently, however, it was found by Snyder & Cox (1966) and Barnett & Wilkerson (1967) that the growth rate of waves observed in ocean is roughly one order of magnitude greater than that predicted by Miles theory. Judging from the discrepancy, Miles (1967) conjected that the wave-induced turbulent Reynolds stresses, although neglected in his laminar model, are not negligible for the long gravity-waves in ocean (in this respect, detailed analytical discussions are given by Phillips (1966, § 4.3 & § 4.6)). He also stated that the advanced theory including the turbulent Reynolds stresses could not be accomplished without more detailed experimental data of wind.

On the other hand, Stewart (1967) submitted some doubts about the whole concept due to Miles (1957) showing that no significant wave-like air motion is indicated by a group of wind velocity spectra observed a short distance above the wave crests by Smith (1967). Alternatively Stewart proposed new ideas involving the effect of the turbulence in wind, and of different flow configurations from that proposed by Miles. He, however, could not check the validity of those ideas for lack of observed data and pointed out that there was a crying need for measurements in the air below the level of the wave crests.

Recently use is being made of a mechanical wave maker for the laboratory measurements of the growth rate of the longer gravity-waves (Mitsuyasu, 1966) or the wind field over those waves (Shemdin & Hsu, 1966, 1967). Generally in a wind-wave tunnel may be presumed a relatively large amount of wave-induced fluctuations in the wind velocities over those waves of considerable height. In the fields, wind spectra and wind shear stresses have already been observed over waves with various instruments by a group at University of British Columbia, that is Pond *et al* (1963), Pond *et al* (1966), Smith (1967), Weiler & Burling (1967), etc. Meanwhile in the laboratory as far as the authors know, no experimental data has been published yet on the velocity fluctuations of wind over water waves.

This paper is concerned with the wind velocity fluctuations measured at several fixed point over waves in a wind-wave tunnel. Actually we measured the longitudinal velocity spectra both over the long periodic waves generated by a wave maker and superposed by smaller wind waves and over the corresponding wind waves only by the use of a hot-wire anemometer and digital procedures. In order to find out the direct relations between those velocity fluctuations and waves, we measured further the cross-spectra between the two. The following results may not necessarily supply what was requested by Miles nor

Stewart. But in this report we discuss mainly the properties of wave-induced velocity fluctuations in wind above wave crests, also paying some attention to the differences between the wind-wave tunnel and the field measurements.

2. Experimental Equipment and Procedures

2.1 General Description of Experiments

The experiments reported below were conducted in a wind-wave tunnel, whose sketch is shown in Fig. 1. The test section is 150 cm wide, 130 cm high and 2850 cm long. The side walls and most of the ceiling consist of glass plates.

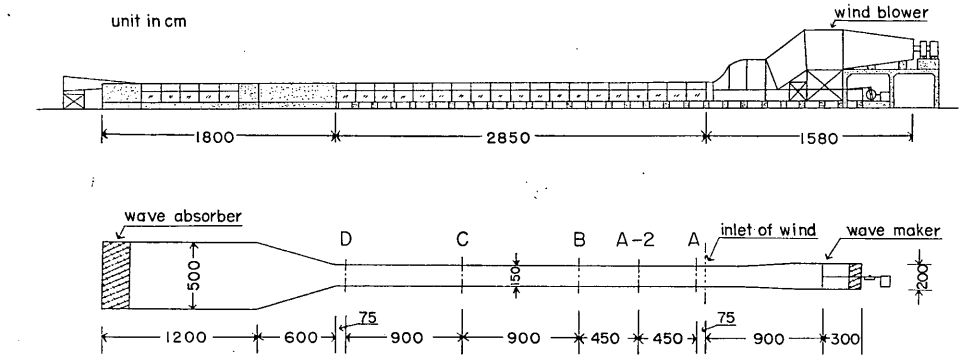

Fig. 1 Wind-Wave Tunnel

On the leeward of the uniform test section, is the enlarged part as seen in Fig. 1. At the leeward end of this part, wind is diffused and surface waves are dissipated by a slope of pebbles and stainless steel turnings. At the windward end of the waterway, a mechanical wave maker of piston type is equipped to generate regular waves of relatively long period. On the windward side of the test section is situated a wind blower, where air flow is controlled by the speed (rpm) of an axial fan driven by a 75 HP variable-speed motor. Large scale turbulence and rotation of air flow caused by the fan are removed through guide vanes, a fine mesh screen and honeycombs. Air flow is supplied the tunnel horizontally at the inlet where is an adjustable-height guide plate as shown in Fig. 2. A maximum mean wind speed is nearly 30 m/sec for the water depth of 50 cm. At the Section A, 75 cm leeward of the inlet, the wind speed distribution is quite uniform and the turbulence level $\sqrt{\overline{u'^2}}/U$ (u'= velocity fluctuations, U=mean wind speed) is nearly 0.40%.

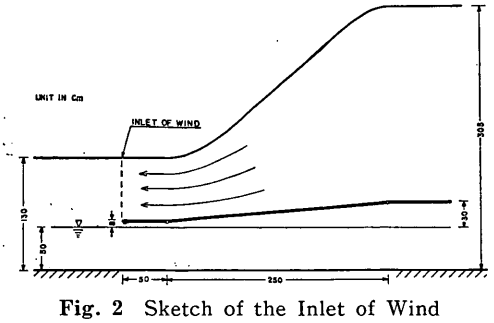

Fig. 2 Sketch of the Inlet of Wind

In the present study we used the wind flower at rpm 200 only. rpm indicates the number of revolution of flower's fan per minute. The depth of water was 50 cm and the corresponding mean wind speed at Section A was nearly 5.6

m/sec. We fixed the stroke and speed of the wave maker so that it always generated the identical waves with period $T=1.60$ seconds and height $H\fallingdotseq 5.6$ cm (at C Section of 18.75 m fetch). Measurements were made at Section C of wind velocity fluctuations mainly over two kinds of waves. The first ones consisted of long periodic waves generated by the wave maker at the condition mentioned above and smaller wind waves generated by wind at rpm 200. We call these waves '*superposed long waves*' in the following. The second waves were the ones generated only by wind at rpm 200. Those waves are shown visually in Fig. 3.

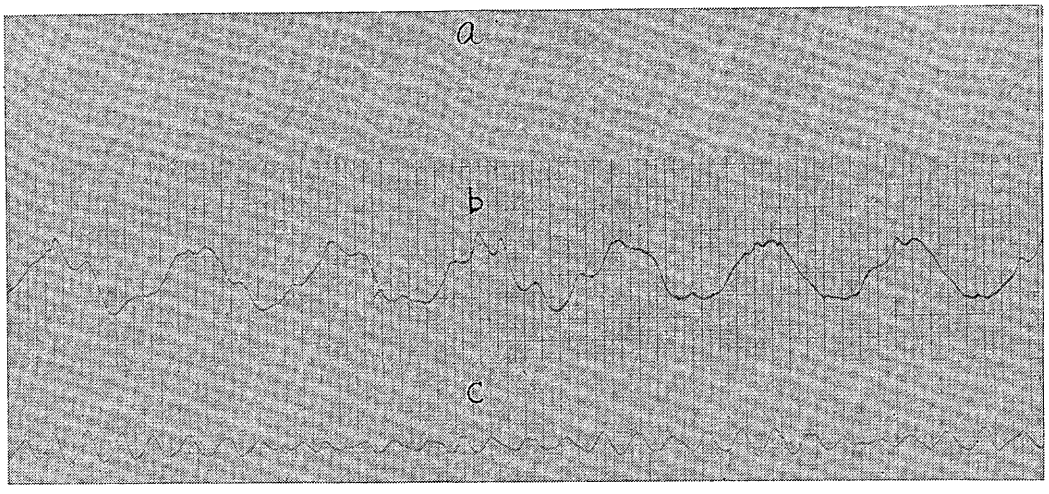

Fig. 3 Wave Records

(**a**: original long waves, **b**: superposed long waves, **c**: wind waves only)

It was necessary to keep the guide plate (Fig. 2) at the height of nearly 8 cm above the still water level in order to pass the mechanically generated waves freely. The clearance was retained also for the case of wind waves only. The effect of this clearance on air flow will be discussed later (§ 3.1).

Velocity fluctuations data obtained with a hot wire system, together with wave data if necessary, were recorded digitally on a magnetic tape by means of a digital data recorder. A digital computer TOSBAC-3400 of our Institute was used for data reduction and numerical computation of auto- and cross-spectra.

2.2 Hot-Wire Anemometer and Other Instruments

The hot-wire anemometer used in this study is a constant temperature compensated unit with a high frequency response, reported by the manufacturer (Nihon Kagaku Kogyo Co.), of 0~50 KC. A hot-wire element consists of a tungsten wire of $5\mu\phi$ and 1 mm length, a pair of prong and an insulator body with two contacts (Fig. 4). This element is fixed to the support of 8 mmϕ, and is alined so that the longitudinal axis of hot-wire is both horizontal and normal to the direction of mean flow.

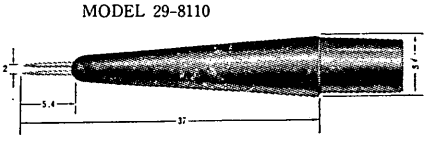

Fig. 4 Hot-Wire Element

The constant temperature compensated anemometer measures the rate of heat

transfer between the constant temperature hot-wire and the surrounding environment. This heat transfer is just equal to the electrical power input to the hot-wire. The heat transfer relation for a wire in cross flow, which has been studied by many investigators, can be written to a good approximation

$$\frac{E^2}{R}=[A+BV^n](T_s-T_e)\,, \tag{2.1}$$

where E=the instantaneous output voltage from the anemometer, V=the instantaneous velocity normal to the hot-wire, R=the electrical resistance of the hot-wire in operation, T_s=the hot-wire surface temperature, T_e=the environment temperature, A and B=coefficients obtained from a calibration, and n is a constant, which is usually taken as 1/2* after King's Law (Hinze, 1959, p. 79). V is expressed as

$$V=\sqrt{(U+u')^2+w'^2}\,, \tag{2.2}$$

where U is the mean wind velocity, u' is the fluctuating component of velocity parallel to mean flow (x-direction), and w' is the vertical velocity fluctuation. Usually we can put $u'\ll U$ and $w'\ll U$, and expanding (2.2) in a power series yields

$$V=U\left(1+\frac{u'}{U}+\frac{w'^2}{2U^2}-\frac{u'w'^2}{2U^3}+\cdots\right)\fallingdotseq U+u'\,. \tag{2.3}$$

For a given hot-wire operating temperature and a constant enviroment temperature, (2.1) can be re-written, taking n as 1/2

$$V=\alpha_1(E^2-E_0^2)^2\,, \tag{2.4}$$

where

$$\alpha_1=[B(T_s-T_e)]^{-1/2}\,,$$

and E_0 is the output voltage at zero velocity. Using the relations (2.3) and (2.4), we can obtain u' from the instantaneous voltage E. However, it is inconvenient because V is proportional to E^4. Therefore we used a linearizer in order to get the voltage directly proportional to V; we take the voltage E as the input to the linearizer which produces the output voltage M given by

$$M=\beta_1(E^2-E_0^2)^2\,, \tag{2.5}$$

where β_1 is a constant depending on the setting conditions. Eqs. (2.4) and (2.5) give a simple relation

$$V=K_1M\,, \tag{2.6}$$

where K_1 is a constant ($=\alpha_1/\beta_1$). Consequently, we can easily obtain u' from the fluctuating component of linearizer output voltage m' by

$$u'=K_1m'\,. \tag{2.7}$$

* Collis & Williams (1959) obtained $n=0.45$ for $0.02<Re<44$, and $n=0.51$ for $44<Re<140$, where Re is the Reynolds number referred to the hot-wire diameter. Re in the present measurements belongs to the former range.

The coefficient K_1 was obtained from the calibration carried out just before each day measurements by the following procedure. We placed a hot-wire and a pitot static tube side by side at the center (z=40 cm) of the tunnel cross-sectional area at C Section, where the turbulence level was fairly low. For four or five different rpm of the wind blower, the mean wind speeds $\bar{V}$ ($=U$) were measured by using the pitot static tube in conjuction with a manometer of Göttingen type, and also the linearizer output voltages were recorded with the digital data recorder described below, the means $\bar{M}$ being evaluated. The calibration curves between $\bar{M}$ and $\bar{V}$ thus obtained, one of which is shown in Fig. 5, were very linear except near the origin. K_1 was obtained from the slope of the calibration line.

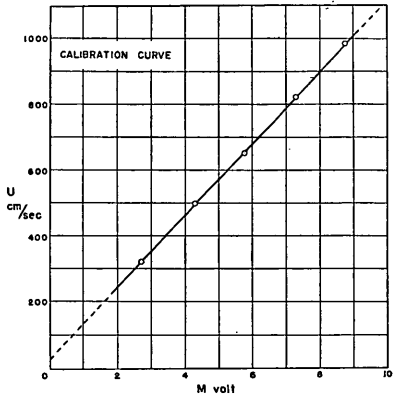

Fig. 5 Calibration Curve for Hot-Wire

The wave heights were measured by using a capacitance-type wave gauge and a capacitance bridge. The wave-height sensor is a polyvinyl-formal wire of 0.8 mm outside diameter and 30 cm length, which is mounted on a usual frame but differently as seen from Fig. 7. The static calibration of wave heights for each day showed a good linear response.

A digital data recorder (DATAC-2000, Iwasaki Commun. Instr. Co.) was used for recording the output voltages from the linearizer and the capacitance wave meter. The recorder has three input channels now, but the number of the channel can be increased up to six. After being pre-amplified, if necessary, the input analogue data are converted into digital quantities and are recorded on a magnetic tape of 1/2 inch width in a format fitted to the digital computer (compatible with IBM 729-2~4 MT handler). The significant figures of the A-D converter are three (−999~+999) and the converting time is less than 150 μ seconds. The sampling frequencies are from 45 c/s to 1440 c/s for one channel use. The quasi-simultaneous sampling is also possible, where the time lag between the successive channels is 150 μ seconds. It was naturally used for cross-spectra measurements.

In order to use the digital data recorder effectively, the DC component of the linearizer output voltage was first eliminated by means of a DC-cut filter, and only fluctuating component was fed to the recorder. This filter caused only negligible attenuation of voltage at frequencies higher than 0.05 c/s. A quantitative check of this filter will be shown in § 2.4.

2.3 Measurements of Wind Velocity Spectra

Wind velocity fluctuations usually have very wide frequency components. Therefore a digital method for obtaining the wind velocity spectra may not necessarily advantageous, and in fact most of measurements of those spectra have been made using analogue techniques. However, the digital method of analysis is easier than the analogue one in eliminating the low frequency distortion. The digital method was typically used by Raichlen (1967) in measuring the turbulence in water, not in wind.

In the present study, the above mentioned digital data recorder and digital computer were available at hand so that we took the digital course in measuring the wind velocity spectra. The digital computations were performed following the procedure of Blackman & Tukey (1958), which is identical with that of auto-spectrum estimation in the cross-spectral analysis (see § 2.4). Since there was a limit of 1/1440 second in the available sampling intervals of the digital recorder, we could evaluate only the spectral densities at frequencies up to 720 c/s. We were, however, rather interested in the low frequency component in order to detect the wave-induced velocity fluctuations. For this purpose, since the frequency of superposed long waves was 0.625 c/s, it was necessary to take the frequency resolution less than 0.1 c/s. In the digital estimation of spectrum, the frequency resolution Δf and the holding frequency f_N are given, respectively, by

$$\Delta f=\frac{1}{2\Delta t h}, \tag{2.7}$$

$$f_N=\frac{1}{2\Delta t}, \tag{2.8}$$

where h is number of maximum lag and Δt is data sampling interval. In practice it is impossible to perform the computation with the condition of $\Delta f=0.1$ c/s and $f_N=720$ c/s, because it would take too much time. An alternative procedure is to divide the total frequency range into at least two smaller ranges and to perform a different computation for each divided sub-range. Taking the enough overlap and the computation time into consideration, we practically divided the total frequency range into three sub-ranges: high, middle and low frequency sub-ranges. Δt and h used for each sub-range are shown in Table 1. The data with different Δt for the middle or low sub-range computation were initially made, using the computer, from a long data sampled at $\Delta t=1/1440$ sec. But this procedure turned out to take a considerably long extra time. So that later we repeated the recording successively at the different Δt for each computation.

The total number of data used, N, and the obtained variances of velocity fluctuations, $\overline{u'^2}$, are also included in Table 1. Since we limited the total number as $N\leqq 10{,}000$ for restricting the computation time, the corresponding total period of data for high frequency computations was only about 7 seconds. Nevertheless the values of $\overline{u'^2}$ from these computations were, as seen from Table 1, very consistent with those from other two computations with much longer periods. On one occasion, using the single long data sampled at $\Delta t=1/1440$ sec for $N=95{,}000$ (66.0 sec), and not changing the total period but simply skipping, we estimated $\overline{u'^2}$ for the successively varied Δt such as 1/1440, 1/720, 1/360, 1/180, 1/90 and 1/45 sec. The results of those estimations were consistent within the relative difference of 0.2%. The relative turbulence intensities obtained are nearly 1.7~1.8% at $z=40$ cm and 11~12% at $z=6$ cm. The so-called 'degrees of freedom' of the present spectral computation were within the range of 56~78 except two low frequency cases.

When we estimate the spectral densities from the data sampled at an equal time interval Δt, we must be very careful about aliasing. That is, if the data contain any appreciable power at frequencies greater than the holding frequency f_N given by Eq. (2.8), the estimated spectral densities $P_A(f')$ necessarily become greater than the true densities $P(f')$, as shown by the equation (Blackman &

Tukey 1958, p. 119) below:

$$P_A(f') \fallingdotseq P(f') + \sum_{q=1}^{\infty} \left[P\left(\frac{q}{\Delta t} - f'\right) + P\left(\frac{q}{\Delta t} + f'\right) \right], \tag{2.9}$$

where

$$0 \leqq f' \leqq \frac{1}{2\Delta t}.$$

The terms in the bracket on the right hand side are due to aliasing. This effect of aliasing was very serious for the present computation of low frequency sub-range, since we used no high-cut filter. Of course the larger f_N we use, the smaller the effect of aliasing becomes. The larger f_N, however, necesitates the longer computation time provided we retain the same frequency resolution as well as the degrees of freedom $\left(\fallingdotseq \frac{2N}{h}\right)$.

We roughly estimate the magnitude of aliasing for the different values of f_N in the present low frequency computation, taking the spectrum M-8 in Fig. 9 as an example. Assuming the spectral densities for $f \geqq 1.0$ c/s have already been obtained, we take those values as the real densities $P(f)$ in Eq. (2.9). At first, if we take $f_N = 11.25$ c/s ($\Delta t = 2/45$ sec), by Eq. (2.9)

$$\begin{aligned} P_A(1.0) &\fallingdotseq P(1.0) + P(21.5) + P(23.5) + P(44) + P(46) + \cdots \\ &\fallingdotseq P(1.0) + 17.5 \times 2 + 4.5 \times 2 + 2.5 \times 2 + 1.7 \times 2 + 1.0 \times 2 + 0.9 \times 2 \\ &\qquad + 0.68 \times 2 + 0.55 \times 2 + \cdots \\ &= P(1.0) + 58.7 + \cdots \qquad (\mathrm{cm}^2 \cdot \mathrm{sec}^{-1}). \end{aligned}$$

Since $P(1.0) \fallingdotseq 530$ $(\mathrm{cm}^2 \cdot \mathrm{sec}^{-1})$, the magnitude of aliasing is roughly 11%. For $f_N = 22.5$ c/s, in the same way

$$P_A(1.0) \fallingdotseq P(1.0) + 17.5,$$

and the magnitude of aliasing is nearly 3.3%. For $f_N = 45$ c/s, it is nearly 1.0%.

2.4 Measurements of Cross Spectra between Wind and Waves

In order to investigate the relations between the corresponding frequency components of two random time series $x(t)$ and $y(t)$, it is convenient to estimate the cross-spectrum between the two. As the power spectrum for a single time series is the Fourier transform of the autocorrelation, so the cross-spectral denity $G_{xy}(f)$ for two time series $x(t)$ and $y(t)$ is the Fourier transform of the cross-correlation $R_{xy}(\tau)$. That is, for the infinite continuous time series

$$G_{xy}(f) = \int_{-\infty}^{\infty} R_{xy}(\tau) e^{-i2\pi f\tau} \, d\tau, \tag{2.10}$$

where

$$R_{xy}(\tau) = \lim_{T \to \infty} \frac{1}{2T} \int_{-T}^{T} x(t) \cdot y(t+\tau) \, dt. \tag{2.11}$$

Since $R_{xy}(\tau)$ is not an even function of τ, $G_{xy}(f)$ cannot be expressed as a cosine transform like the auto-spectrum but expressed in a complex form:

$$G_{xy}(f)=C_{xy}(f)-iQ_{xy}(f)\,, \tag{2.12}$$

where $C_{xy}(f)$ and $Q_{xy}(f)$ are called the *cospectrum* and *quadrature spectrum*, respectively, and given by

$$\left.\begin{aligned} C_{xy}(f)&=2\int_0^\infty \alpha_{xy}(\tau)\cos 2\pi f\tau\, d\tau\,,\\ Q_{xy}(f)&=2\int_0^\infty \beta_{xy}(\tau)\sin 2\pi f\tau\, d\tau\,, \end{aligned}\right\} \tag{2.13}$$

where

$$\left.\begin{aligned} \alpha_{xy}(\tau)&=\frac{1}{2}[R_{xy}(\tau)+R_{xy}(-\tau)]\,,\\ \beta_{xy}(\tau)&=\frac{1}{2}[R_{xy}(\tau)-R_{xy}(-\tau)]\,. \end{aligned}\right\} \tag{2.14}$$

$G_{xy}(f)$ can also be expressed in complex polar notation:

$$G_{xy}(f)=Z_{xy}(f)e^{-i\theta(f)}\,, \tag{2.15}$$

where the magnitude $Z_{xy}(f)$ and the phase angle $\theta(f)$ are related to $C_{xy}(f)$ and $Q_{xy}(f)$ by

$$\left.\begin{aligned} Z_{xy}(f)&=\sqrt{C_{xy}^2(f)+Q_{xy}^2(f)}\,,\\ \tan\theta(f)&=\frac{Q_{xy}(f)}{C_{xy}(f)}\,. \end{aligned}\right\} \tag{2.16}$$

The coherence $\gamma_{xy}^2(f)$, which is a measure of the correlation between $x(t)$ and $y(t)$ at the frequency f, is given by

$$\gamma_{xy}^2(f)=\frac{C_{xy}^2(f)+Q_{xy}^2(f)}{P_{xx}(f)\cdot P_{yy}(f)}\,,$$

where $P_{xx}(f)$ and $P_{yy}(f)$ are the auto-spectrum of $x(t)$ and $y(t)$, respectively. The coherence theoretically should satisfy $0\leqq\gamma_{xy}^2(f)\leqq 1$ for all f (e.g. Jenkins, 1963). When $\gamma_{xy}^2(f)=0$ at a particular frequency, $x(t)$ and $y(t)$ are said to be uncorrelated at that frequency. If $x(t)$ and $y(t)$ are statistically independent, then $\gamma_{xy}^2(f)=0$ for all frequencies. With finite records, however, it has random values. When $x(t)$ and $y(t)$ are identical but there is a time lag in one record corresponding to $\theta(f)$, then $\gamma_{xy}^2(f)=1$ for all f.

These cross-spectral analyses were used, in the present study, in order to investigate the direct relations between wind velocity fluctuations u' and water surface displacements η at the corresponding frequencies. The numerical computations by means of the digital computer were performed by the procedure as follows.

We take u' as the x-record and η as the y-record; $x_1, x_2, \cdots, x_N$ and $y_1, \cdots,$

y_N represent the total N data of u' and η, respectively, sampled at the time interval Δt. The first step is the computations of the sample means $\bar{x}$ and $\bar{y}$, namely

$$\left.\begin{aligned}\bar{x}&=\frac{1}{N}\sum_{j=1}^{N}x_j\,,\\ \bar{y}&=\frac{1}{N}\sum_{j=1}^{N}y_j\,.\end{aligned}\right\} \tag{2.18}$$

The auto-correlations, $\bar{R}_x$ and $\bar{R}_y$, of the x- and y-data, respectively, are given by

$$\left.\begin{aligned}\bar{R}_x(l)&=\frac{1}{N-l}\sum_{j=1}^{N-l}(x_j-\bar{x})(x_{j+l}-\bar{x})\,,\\ \bar{R}_y(l)&=\frac{1}{N-l}\sum_{j=1}^{N-l}(y_j-\bar{y})(y_{j+l}-\bar{y})\,,\end{aligned}\right\} \tag{2.19}$$

$$l=0,1,2,\cdots,h\,.$$

The cross-correlations, $\bar{R}_{xy}(l)$ and $\bar{R}_{xy}(-l)$, of the two data are given by

$$\left.\begin{aligned}\bar{R}_{xy}(l)&=\frac{1}{N-l}\sum_{j=1}^{N-l}(x_j-\bar{x})(y_{j+l}-\bar{y})\,,\\ \bar{R}_{xy}(-l)&=\frac{1}{N-l}\sum_{j=1}^{N-1}(x_{j+l}-\bar{x})(y_j-\bar{y})\,,\end{aligned}\right\} \tag{2.20}$$

$$l=0,1,2,\cdots,h\,.$$

The raw estimate of x auto-spectrum (one-sided form), $\bar{P}_{xx}(m)$, is obtained by

$$\bar{P}_{xx}(m)=2\Delta t\left[\bar{R}_x(0)+2\sum_{l=1}^{h-1}\bar{R}_x(l)\cos\left(\frac{\pi ml}{h}\right)+(-1)^m\bar{R}_x(h)\right], \tag{2.21}$$

$$m=0,1,2,\cdots,h\,.$$

The raw estimate of y auto-spectrum, $\bar{P}_{yy}(m)$ is obtained using y in place of x in the above equation. Corresponding to Eq. (2.13), the raw estimates of the cross-spectrum for the discrete data x_j and y_j are given by*

$$\left.\begin{aligned}\bar{C}_{xy}(m)&=2\Delta t\left[S^+(0)+2\sum_{l=1}^{h-1}S^+(l)\cos\left(\frac{\pi ml}{h}\right)+(-1)^mS^+(h)\right],\\ \bar{Q}_{xy}(m)&=4\Delta t\sum_{l=1}^{h-1}S^-(l)\sin\left(\frac{\pi ml}{h}\right),\end{aligned}\right\} \tag{2.22}$$

where

---

* If the maximum of the cross-correlation $\bar{R}_{xy}(l)$ occurs at the appreciable value of l, say $l=l_1$, the origin of the cross-correlation should be shifted to $l=l_1$, in order to avoid the distortion in computing the cross-spectrum (e.g. see Bendat & Piersol 1966, p. 302). However, this is not the case in our computations as seen from Figs. 12 and 13.

$$\left.\begin{aligned} S^{+}(l)&=\frac{1}{2}[\bar{R}_{xy}(l)+\bar{R}_{xy}(-l)]\,,\\ S^{-}(l)&=\frac{1}{2}[\bar{R}_{xy}(l)-\bar{R}_{xy}(-l)]\,,\\ l&=0,1,2,\cdots,h\,. \end{aligned}\right\} \tag{2.23}$$

The auto- and cross-spectral densities are obtained by smoothing these raw estimates with the window (a_{-1}, a_0, a_1), respectively. For instance, the auto-spectral densities of x data, $\hat{P}_{xx}(m)$, are given by

$$\left.\begin{aligned} \hat{P}_{xx}(m)&=a_{-1}\bar{P}_{xx}(m-1)+a_0\bar{P}_{xx}(m)+a_1\bar{P}_{xx}(m+1)\\ &\qquad \text{for}\quad m=1,2,\cdots,h-1\,,\\ \hat{P}_{xx}(0)&=a_0\bar{P}_{xx}(0)+(a_{-1}+a_1)\bar{P}_{xx}(1)\,,\\ \hat{P}_{xx}(h)&=a_0\bar{P}_{xx}(h)+(a_{-1}+a_1)\bar{P}_{xx}(h-1)\,. \end{aligned}\right\} \tag{2.24}$$

$\hat{P}_{yy}(m)$, $\hat{C}_{xy}(m)$ and $\hat{Q}_{xy}(m)$ are obtained in the same ways, where a_{-1}, a_0 and a_1 are given as follows:

	a_0	$a_1=a_{-1}$
Akaike's W_1	0.5132	0.2434
Hamming	0.54	0.23
Hanning	0.50	0.25

In the estimation of the wind-velocity spectra described in the preceding section, only the Hamming window was used. While in the cross-spectral computations, all three windows shown above were used successively, and it was found that the three windows gave essentially the same results. The spectral densities and associated quantities presented in the later figures are all due to Hamming.

The coherence $\hat{\gamma}^2(m)$ and the phase difference $\hat{\theta}(m)$ between the m-th components of x and y are given by the following equations.

$$\hat{\gamma}^2(m)=\frac{\hat{C}_{xy}^2(m)+\hat{Q}_{xy}^2(m)}{\hat{P}_{xx}(m)\cdot\hat{P}_{yy}(m)}\,, \tag{2.25}$$

$$\left.\begin{aligned} \hat{\theta}(m)&=\tan^{-1}\left[\frac{\hat{Q}_{xy}(m)}{\hat{C}_{xy}(m)}\right]+\frac{\pi}{2}[1-\operatorname{sgn}(\hat{C}_{xy}(m))]\operatorname{sgn}(\hat{Q}_{xy}(m))\\ &\qquad\qquad \text{for}\quad \hat{C}_{xy}(m)\neq 0\\ &=\frac{\pi}{2}\operatorname{sgn}(\hat{Q}_{xy}(m)) \qquad \text{for}\quad \hat{C}_{xy}(m)=0\,, \end{aligned}\right\} \tag{2.26}$$

where by definition

$$\operatorname{sgn}(s)=\begin{cases} 1 & (s>0)\\ 0 & (s=0)\\ -1 & (s<0)\,. \end{cases}$$

$\hat{\theta}$ obtained from the above relation represents the phase lag of the y-record (wave in our case) relative to the x-record (wind).

Since the wind and wave data were recorded by the quasi-simultaneous sampling, there existed a time lag of 150 μsec between the corresponding x_j and y_j. The effect of this time lag, however, was guite negligible because the turbulence level at the frequencies greater than 1000 or 2000 c/s was much lower than at the low frequencies, which we were concerned with, as seen from the wind-velocity spectra in Figs. 9 and 11. Those data were sampled at the time intervals, $\Delta t=2/45$ sec for the case of superposed long waves and $\Delta t=1/30$ sec (partially, 1/45 sec) for the case of wind waves only. We used no high-cut filter for the cross-spectra measurements either, so that some aliasing must have been included. Although we did not evaluate the magnitude of aliasing for cross-spectra, it was expected to be considerably smaller than that for auto-spectra (which is shown in § 2.3), since the wave data contain no significant frequency component for $f>10$ c/s.

The DC-cut filter was also used in recording the wind-velocity fluctuations for cross-spectra. Of course we took care to record the u' and η data with the correct relative phase. Once we recorded the linearizer output voltages, which were taken at $z=6$ cm over the superposed long waves, both using and without using the DC-cut filter quasi-simultaneously by the parallel connection. Using these two data we carried out a test cross-spectral computation with the same condition as the real runs; $\Delta t=2/45$, $N=4500$ and $h=225$, where x_j were the total voltages (without the filter) and y_j were the fluctuating voltages (through the filter). The raw data corresponding to u' were within ± 80 at most. The estimated variances (not multiplied by a conversion factor) were $(\overline{u'^2})_x=1661.9$ and $(\overline{u'^2})_y=1621.7$, so that the relative error was 2.4%. The relative errors between the each auto-spectral densities, $(\hat{P}_{xx}(f)-\hat{P}_{yy}(f))/\hat{P}_{xx}(f)$, and the phase lag, $\hat{\theta}(f)$, are shown in Fig. 6. Although there is considerable scatter, the relative errors are nearly 2 or 3% at the frequencies lower than 3.0 c/s. The correspond-

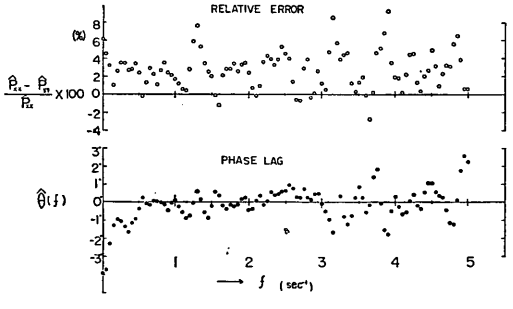

Fig. 6 Results of Filter Test

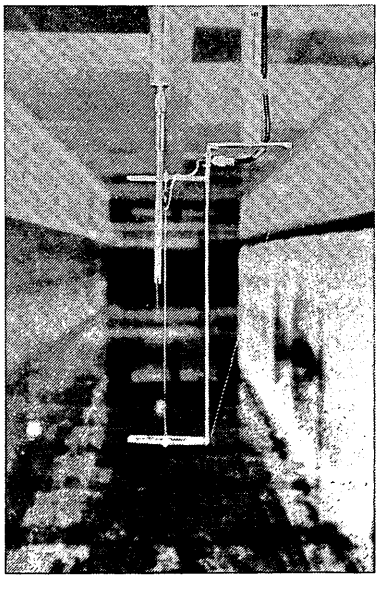

Fig. 7 Configulation of Hot-Wire Probe and Wave Gauge

ing coherences were always larger than 0.999. It was thus found that the DC-cut filter caused the voltage attenuation of nearly 1.6% and a quite negligible phase shift.

Special efforts were made for the installation of the hot-wire probe and the wave-gauge. It was desirable to install them in a vertical line, but this was impossible. Though initially we placed the wave gauge a small distance downwind of the hot-wire probe, in the later runs reported here we placed them side by side nearly 0.9 cm apart with no longitudinal distance. The configuration is shown in Fig. 7.

3. Results and Discussion

3.1 Mean Wind Data

Mean wind profiles at Section C under the present experimental conditions, which were measured using a pitot static tube, are shown in Fig. 8, where the profile A is for the case of superposed long waves and the profiles B–1 and B–2 are for wind waves only. As mentioned earlier, the guide plate at the inlet of wind was placed nearly 8 cm above the still water level. In order to examine the effect of the clearance, the wind profiles for the wind waves only were also measured by placing the guide plate just at the still water level. Roughly speaking, the clearance brought the outer portion of the wind profiles close to the extension of the inner portion for the short fetches such as Section A–2 or B in Fig. 1. However, as far as the profiles at Section C are concerned, there was found only little effect. That is, the profiles B–1 and B–2 are typical of the ordinary velocity profiles which we have obtained over relatively small wind waves in our wind-wave tunnel. As can be seen from Fig. 8, there is a definte difference between the wind profile over the superposed long waves and that over the wind waves only, and the similar difference was also found by Shemdin & Hsu (1966). The profile over the superposed long waves, on a semi-log plot, is fairly linear, and it makes the approximation by the so-called log-law (3.1) attractive. On the other hand, the profiles over the wind waves only are not straight. They have the distinct outer portion of the boundary layer similar to that over the fixed rough surface in a wind-tunnel (e.g. Clauser, 1956). It has already been established that the inner portion of the mean wind profile over the fixed rough surface is represented as

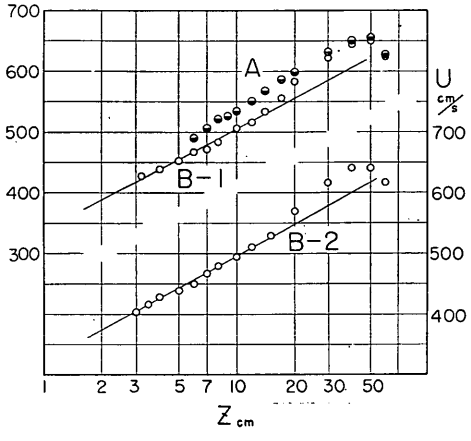

Fig. 8 Mean Wind Profiles at Section C
(A: over superposed long waves, B-1 and B-2: over wind waves only)

$$U(z)=5.75u_* \log \frac{z}{z_0}, \tag{3.1}$$

where $U(z)$ is the mean wind speed at the height z, u_* the friction velocity and z_0 the roughness length. It is a question indeed whether the relation (3.1) can be applied for any portion of those wind profiles over the wind waves only. If, however, we apply (3.1) to the lower portion of the profiles B-1 and B-2 (straight lines) as well as the profile A, the values of u_* and z_0 for each profile are obtained as follows: (A) $u_*=34.8$ cm/sec, $z_0=1.9\times10^{-2}$; (B-1) $u_*=29.0$ cm/sec, $z_0=0.92\times10^{-2}$; (B-2) $u_*=30.1$ cm/sec, $z_0=1.0\times10^{-2}$.

3.2 Spectra of Wind Velocity

Data relevant to the measurements and computations of longitudinal wind velocity spectra are listed in Table 1. Figs. 9 and 10 show the obtained spectra at heights $z=6$, 15 and 40 cm for the case of superposed long waves, and Fig. 11 shows the spectra at heights $z=6$ and 40 cm for the case of wind waves only.

Table-1 List of Measurements and Computations of Wind Velocity Spectra

Wave	Height (cm)	Spectrum No.	Data No.	Δt	N	h	$\overline{u'^2}$ (cm^2·sec^{-2})	Date of Exp.
Superposed Long Waves	$z=6$	M-8	Y1381	1/45	8,400	225	2.66×10^3	7/23
			Y1382	1/360	10,000	360	2.89×10^3	
			Y1383	1/1,440	10,000	360	2.79×10^3	
	$z=15$	M-7	Y1378	1/45	8,800	225	1.46×10^3	7/23
			Y1379	1/360	10,000	360	1.47×10^3	
	$z=40$	M-2	Y1331	1/60	7,350	300	1.44×10^2	6/29
			Y1331	1/360	10,000	360	1.33×10^2	
			Y1332	1/1,440	10,000	288	1.37×10^2	
Wind Waves Only	$z=6$	M-1	Y1329	1/60	6,890	300	3.45×10^3	6/29
			Y1329	1/360	10,000	360	3.19×10^3	
			Y1330	1/1,440	10,000	288	3.66×10^3	
	$z=40$	M-6	Y1376	1/360	10,000	360	1.16×10^2	7/23
			Y1377	1/1,440	10,000	288	1.24×10^2	

In these figures points near the holding frequencies for the low and middle frequency computations are ommitted. Fig. 10 contains only the results of low and middle sub-range computations. Comparing these spectra, one can see that the variation of the spectral densities is of the similar form at frequencies higher than about 10 c/s, though the low frequency parts of the spectra show the different variation.

According to the universal equilibrium theory of Kolmogoroff (Batchelor, 1953), if the Reynolds number of the whole motion is sufficiently large that there exists a range of wave-numbers k:

$$k_0 \ll k \ll k_d, \tag{3.2}$$

where k_0 is the wave-number representative of the energy supply from the mean flow and k_d is the wave-number marking the location of the strongest rate of

dissipation from the spectrum, then there should exist a range of wave-numbers which are locally isotropic but over which the viscous dissipation rate is negligible. In this range, which is called inertial sub-range, the energy spectrum $\phi(k)$

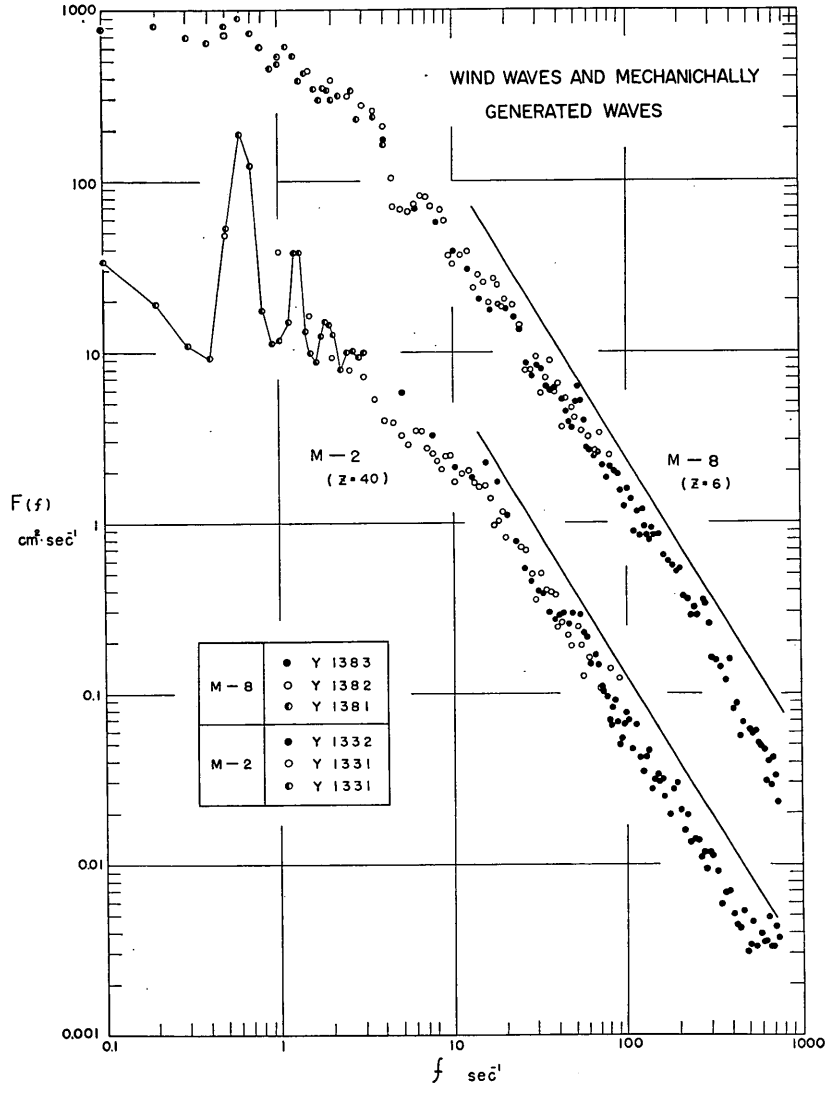

Fig. 9 Wind Velocity Spectra over Superposed Long Waves
(The straight lines have slope −5/3.)

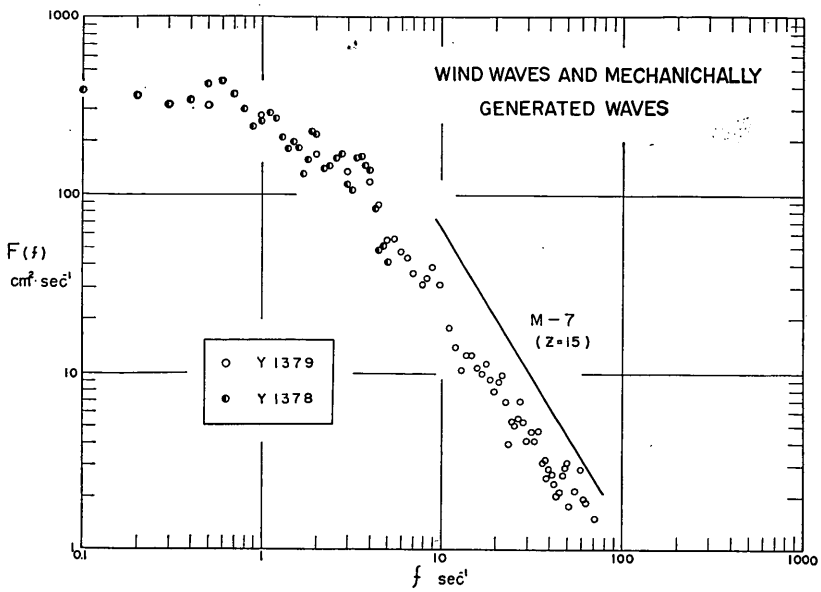

Fig. 10 Wind Velocity Spectra over Superposed Long Waves

of the turbulence is given by

$$\phi(k)=A_K\varepsilon^{2/3}k^{-5/3} \qquad (k_0 \ll k \ll k_d)\,, \tag{3.3}$$

where A_K is an absolute constant and ε is the rate of energy dissipation. The existence of the relation (3.3) has already been demonstrated mainly from the field measurements of turbulence by Grant *et al* (1962), Pond *et al* (1963, 1966), etc. The constant A_K has been found to be nearly 0.48 or 0.49 (Pond *et al*, 1966), and ε can be estimated approximately by

$$\varepsilon=15\nu\int_0^\infty k^2\phi(k)\,dk\,, \tag{3.4}$$

where ν is the kinematic viscosity.

In the present measurements the frequency spectra $F(f)$, not the wave-number spectra $\phi(k)$, were obtained. For large wave-numbers, however, the space and time scales are approximately related by Taylor's hypothesis (for details, see Lumley & Panofsky (1964), p. 56):

$$k=\frac{2\pi f}{U}\,, \tag{3.5}$$

where U is the mean velocity. Therefore we can estimate $\phi(k)$ at high wave-numbers from $F(f)$ by using the above relation.

Since the sufficiently high frequency components of the spectra were not obtained in our measurements, we could not estimate the dissipation rate ε by using (3.4). We can only compare the slopes of obtained spectra with the rela-

tion (3.3). If there exists the inertial sub-range for the turbulence of wind which we measured, the frequency spectra obtained should exhibit variation as $f^{-5/3}$ at high frequencies from (3.3) and (3.5). The straight lines in Figs. 9~11

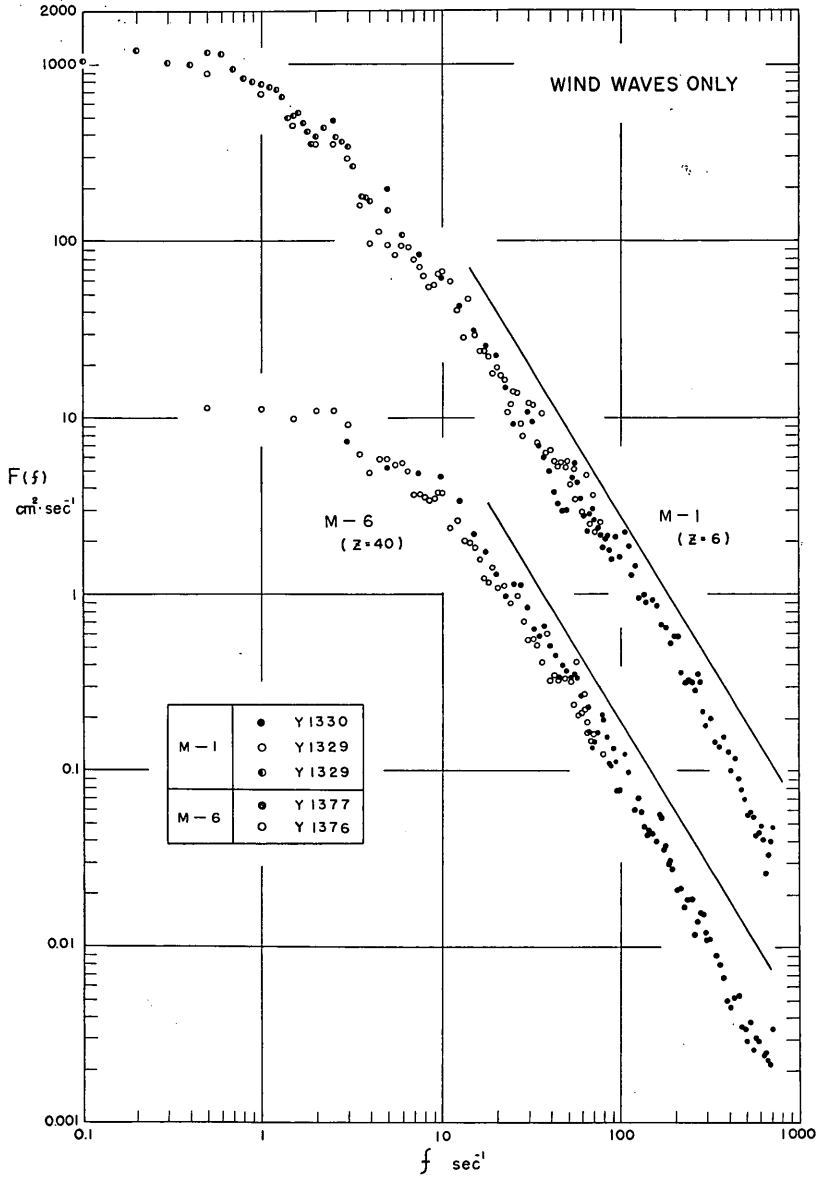

Fig. 11 Wind Velocity Spectra over Wind Waves Only
(The straight lines have slope −5/3.)

have the slope $-5/3$. As can be seen from the figures those spectra are fairly consistent with the variation at the frequency range from about 20 to 350 c/s, although there is a slightly curved (convex) tendency even in this range.

A rough estimate of the limiting wave number for isotropy was found by Pond *et al* (1963) to be

$$k'z \gg 5 . \tag{3.6}$$

Pond *et al* (1963, 1966) also reported that the downwind velocity spectra, observed over the sea, followed very closely the $k^{-5/3}$ law for wave-numbers which are nearly two orders of magnitude lower than the above limit. If we apply the condition (3.6) to our spectra at $z=6$ cm, we cannot expect the velocity fluctuations to be isotropic for nearly $k<2\ \mathrm{cm}^{-1}$, equivalently $f<150$ c/s by (3.5). Thus we find that wind velocity spectra measured in a wind-wave tunnel also exhibit the variation very similar to the $k^{-5/3}$ law for wave-numbers, more or less, much lower than expected from Kolmogoroff's theory.

The spectra in Figs. 9 and 11 show a slight tendency to decrease more rapidly than the slope $-5/3$ at frequencies higher than about 400 c/s but again increase near 720 c/s. This indicates that at frequencies higher than about 400 c/s the viscours dissipation becomes significant and the real spectra decrease more and more rapidly with the frequency than the slope $-5/3$, because the increase near 720 c/s is considered to be simply due to aliasing.

In the low frequency part of the spectra, the variation of densities near the frequency of wave is of special interest. In the case of superposed long waves, the spectrum at $z=6$ cm (M-8 in Fig. 9) has only a small peak near $f=0.6$ c/s corresponding to the frequency $f=0.625$ c/s of the original long wave (cf. the wave spectra in Figs. 25~27). The spectrum at $z=15$ cm (Fig. 10) is much the same as that at $z=6$ cm concerning the peak. The spectrum at $z=40$ cm (M-2 in Fig. 9), however, displays a very dominant peak near $f=0.6$ c/s. These behavior of the spectra may be interpreted as follows. Near the water surface, the fluctuations induced by superposed long waves are fairly comparable with and rather hidden in the irrelevant turbulence which would exist without those long waves. As the height increases to $z=40$ cm, the irrelevant turbulence decays very rapidly, reducing the corresponding spectral dencities at low frequencies by nearly two orders of magnitude, while the wave-induced fluctuations with the frequency of 0.625 c/s become very predominant at $z=40$ cm and the remarkable peak appears near $f=0.6$ c/s in the spectrum for that height. In the case of wind waves only, no significant increase is found of the spectral dencities at the frequencies near 2.5 c/s corresponding to the dominant frequency of wind waves. In this case it may be noticeable that for frequencies lower than about 1 c/s the spectral densities at $z=40$ cm are nearly two orders of magnitude smaller than those at $z=6$ cm, and this also supports the above-stated conjection for the case of superposed long waves. The turbulence level in the boundary layer along a rough wall, measured by Corrsin & Kistler (1954) (also sited by Hinze (1959), Fig. 7-12), decreases nearly linearly with the distance from the wall and tends to zero far outside the layer. Also in the present measurements, which were done at Section C where the boundary layer developed fully, the turbulence level decreased with height, but rather slowly near the water surface and more rapidly above 20 or 30 cm. Anyway this remarkable decreasing of the turbulence

level may be inherent in the wind-tunnel measurements. The direct effect of the waves on the wind velocity fluctuations will be discussed further in the next section.

3.3 Cross-Spectra between Wind and Waves

From a few times trial runs, it was found that there existed more correlation between wind velocity near wave crests and waves as well as more accuracy of the estimation in the case of wind waves only (W) than that of superposed long waves (L). (In this section we use optionally the abbreviations (W) and (L) to designate the two cases as shown above.) Therefore we measured the cross-spectra in case W more minutely and systematically rather than case L.

Let us begin with the case of wind waves only (W). Since there was considerable uncertainty in the estimates of phase lag $\hat{\theta}(f)$, we carried out twice a group of systematic measurements: W-1 (the wind velocity was taken at $z=$ 3, 4, 6, 10 cm) and W-2 (at $z=3, 4, 5, 6$ cm). Conditions for the computation are $N=4500$, $\Delta t=1/30$ sec, $h=150$ for W-1 and $N=7500$, $\Delta t=1/30$ sec, $h=150$ for W-2. The typical cross-correlograms are shown in Figs. 12 and 13. The correlogram in Fig. 12 ($z=3$ cm, W-2) is very similar, though not symmetrical on right and left sides, to the auto-correlogram of wind waves. The cross-correlogram in Fig. 13 has the lower maximum near $\tau=0$ (τ: time delay) than that in Fig. 12, corresponding to the smaller correlation between wind and waves there. Although it is not presented here, the cross-correlogram at $z=15$ cm where the correlation is very small has much smaller and less periodic maximums and minimums, and moreover does not always show the decrease of the envelope with time delay τ like that in Figs. 12 or 13.

Since there is some inconsistency mainly in $\hat{\theta}(f)$ between W-1 and W-2, we present all the results of cross-spectrum measurements, that is co-spectrum $\hat{C}_{xy}(f)$, quad-spectrum $\hat{Q}_{xy}(f)$, phase lag $\hat{\theta}(f)$ and coherence $\hat{\gamma}^2(f)$ together with each wave spectrum $\hat{P}_{yy}(f)$ in Figs. 14~17 (W-1) and Figs. 18~21 (W-2). Both co- and

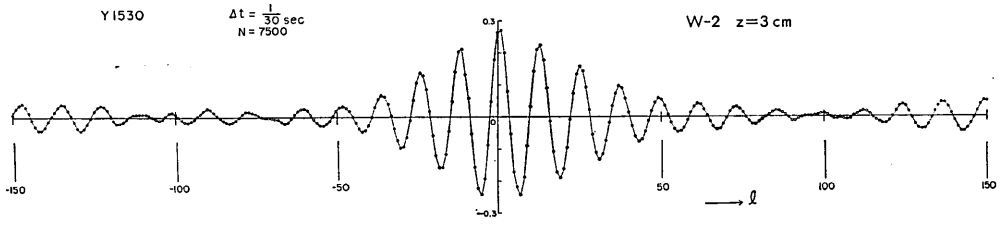

Fig. 12 Cross-Correlogram (wind waves only, $z=3$ cm)

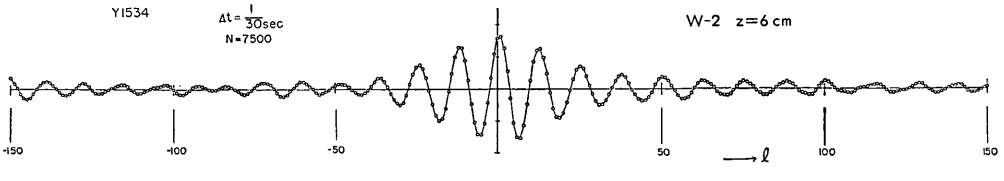

Fig. 13 Cross-Correlogram (wind waves only, $z=6$ cm)

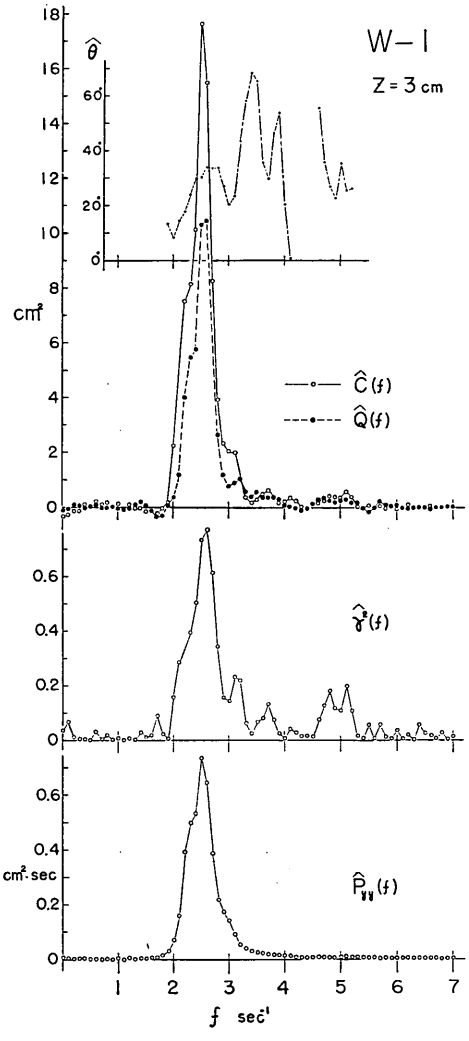

Fig. 14 Cross-Spectrum (wind waves only, z=3 cm)

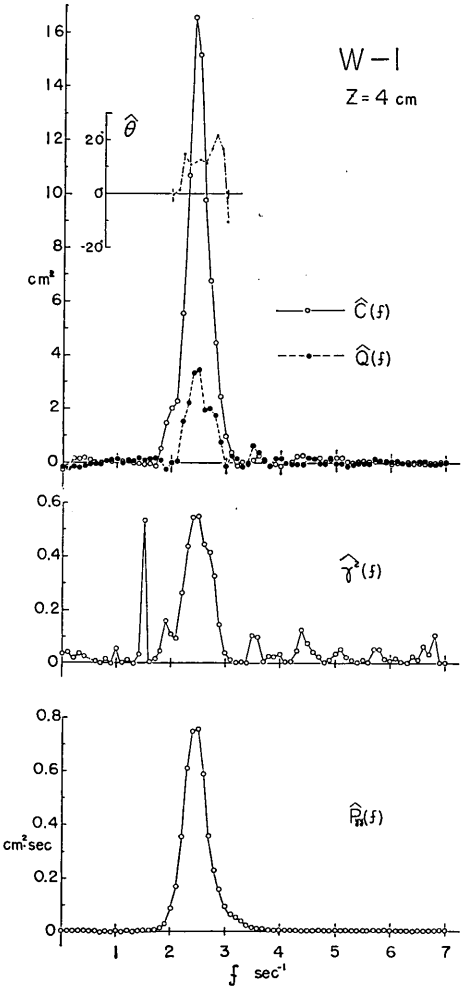

Fig. 15 Cross-Spectrum (wind waves only, z=4 cm)

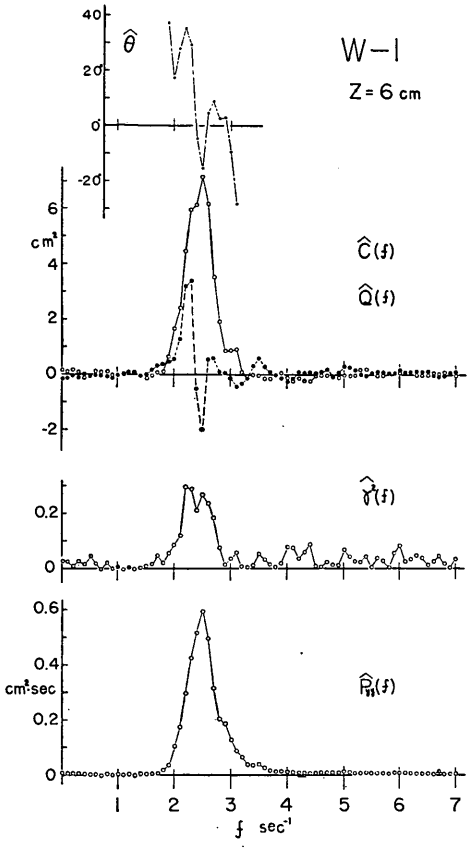

Fig. 16 Cross-Spectrum (wind waves only, z=6 cm)

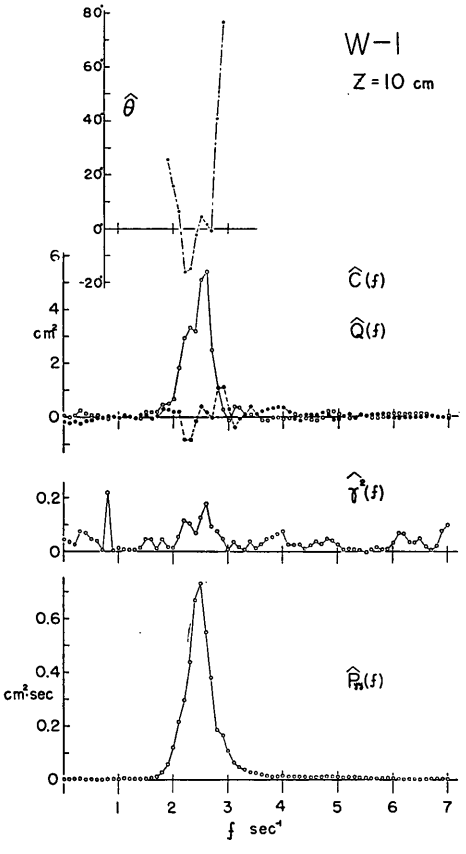

Fig. 17 Cross-Spectrum (wind waves only, z=10 cm)

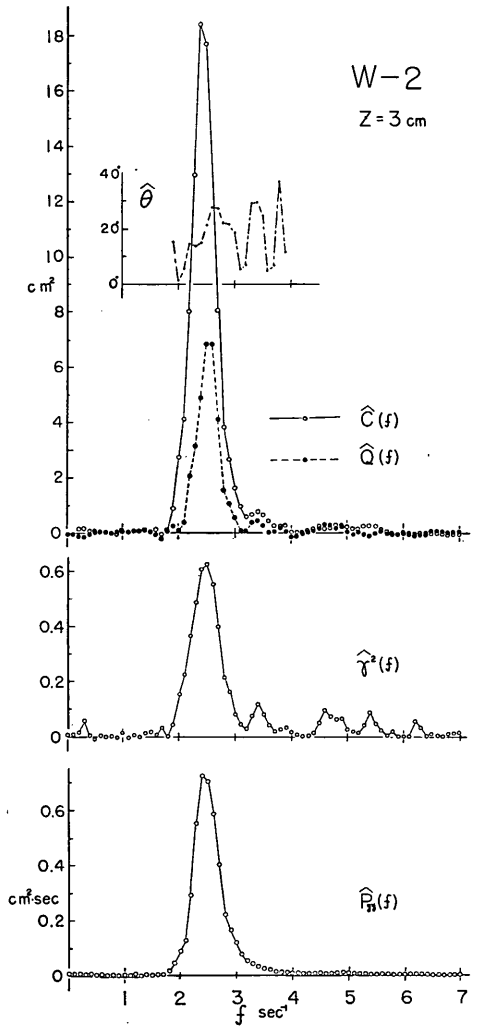

Fig. 18 Cross-Spectrum (wind waves only, z=3 cm)

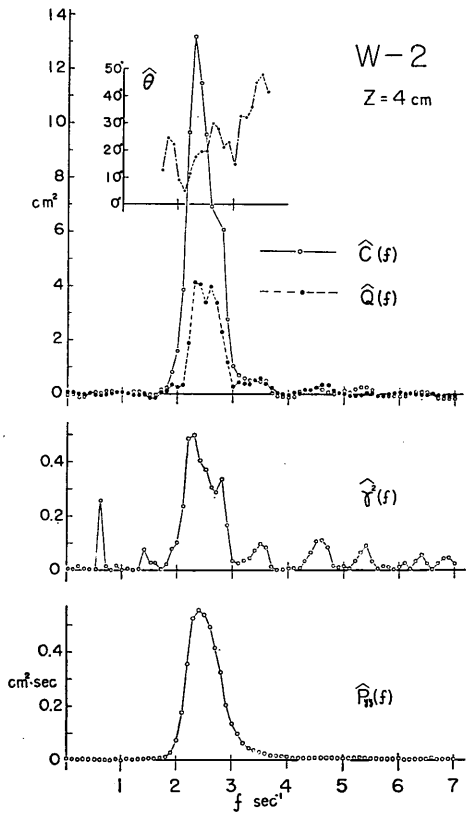

Fig. 19 Cross-Spectrum (wind waves only, z=4 cm)

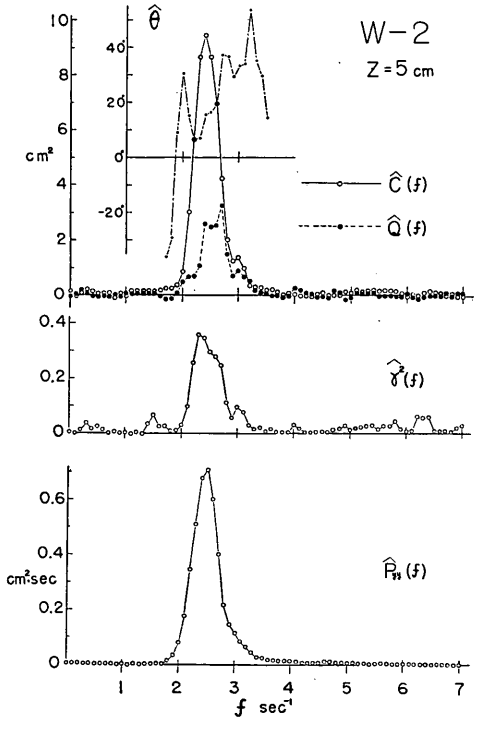

Fig. 20 Cross-Spectrum (wind waves only, z=5 cm)

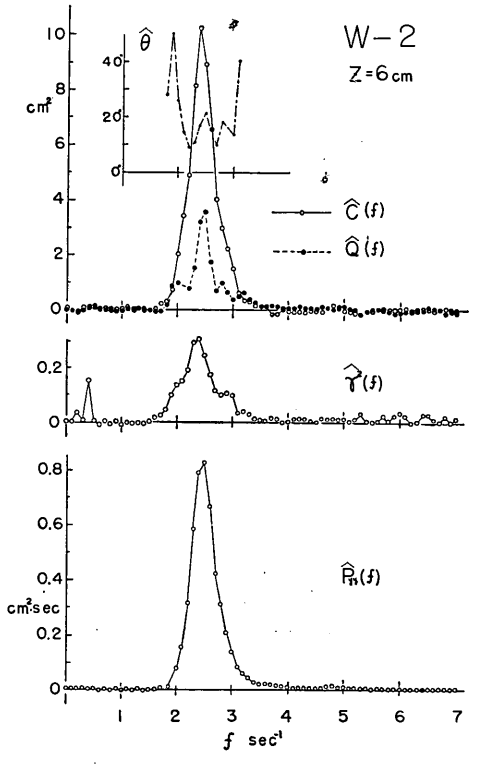

Fig. 21 Cross-Spectrum (wind wave only, z=6 cm)

quad-spectra have a dominant peak at the frequency $f \fallingdotseq 2.5$ c/s of the dominant wave. Especially the peaks of co-spectra are always positive, and the magnitude decreases with height. The coherence also shows a maximum very near the frequency of the dominant wave. The maximum has fairly large values of about 0.7 at z=3 cm and decreases rapidly with height, becoming as small as 0.3 at z=6 cm. The coherence at z=15 cm, which was obtained other time, was smaller than 0.1 for all frequencies.

The phase lags $\hat{\theta}(f)$ are plotted only at the frequencies where the coherences have relatively large values, since $\hat{\theta}(f)$ are very unstable at other frequencies. As can be seen from the figures, the values of phase lag, $\hat{\theta}_W$, at the frequency f=2.4 or 2.5 c/s corresponding to the peak frequency of the wave spectrum are in the range $0° < \hat{\theta}_W < 30°$ except a case shown in Fig. 16 where is seen some singularity in the quad-spectrum. However, there is found a minor inconsistency in $\hat{\theta}_W$ between W-1 and W-2; $\hat{\theta}_W$ in case W-2 varies little with height and is in the range from 15° to 21°, while $\hat{\theta}_W$ in case W-1 shows some tendency to decrease with height. This uncertainty in the estimates of phase lag $\hat{\theta}(f)$ is explained in relation with the coherence $\hat{\gamma}^2(f)$. According to Jenkins (1963), the variance of the estimates of phase lag, $var(\hat{\theta})$, is approximately given by

$$var(\hat{\theta}(f))\sim\frac{h}{2N}\left[\frac{1}{\gamma^2(f)}-1\right], \tag{3.7}$$

where h is number of lag, N total number of data and $\gamma^2(f)$ the true value of coherence. Corresponding to the coherences $\gamma^2=0.9$, 0.7, 0.3 and 0.1, the values in the bracket of Eq. (3.7) very as 0.11, 0.43, 2.3 and 9.0. Thus Eq. (3.7) indicates that the accuracy of the estimate of phase lag is severely dominated by the coherence. Be that as it may, the following are found from the results stated above: the velocity fluctuations which must be induced by waves have the largest intensity at the lowest height ($z=3$ cm) above the wave crests, and they decrease fairly rapidly with height, becoming almost negligible at the height of 15 cm. These wave-induced velocity fluctuations are nearly in phase with waves, the former leading the latter by such a small phase angle as nearly $15°<\theta<30°$.

In connection with the discussion by Stewart (1967), which was mentioned in § 1, we show in Fig. 22 the wind velocity spectra measured at $z=3$ cm in cases W-1 and W-2, where the wave height $H_{1/3}\fallingdotseq2.6$ cm. Those spectra have an obvious peak corresponding to the wave-induced fluctuations at $f\fallingdotseq2.5$ c/s which is just the frequency of the dominant wave. Since, however, the coherence is small at $z=6$ cm, the spectrum discussed in the preceding section (Fig. 11) does not show such a clear peak.

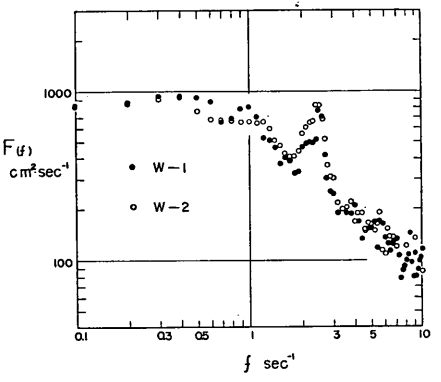

Fig. 22 Wind Velocity Spectra (at $z=3$ cm over wind waves only)

If we represent the wave-perturbed stream function of air flow, for the case of wind profile $U(z)$ ($U''\neq0$), as

$$\Psi=\varphi(z)e^{im_1(x-ct)}, \tag{3.8}$$

where m_1 denotes the wave number and c the phase speed, then φ satisfys the inviscid Orr-Sommerfeld equation:

$$(U-c)(\varphi''-m_1^2\varphi)-U''\varphi=0. \tag{3.9}$$

Hamada (1968) obtained the solution using the approximate method by Lighthill, and gave the horizontal perturbation velocity u_1, for $z>z_c$ (z_c is the critical height, where $U=c$)

$$u_1\simeq\frac{A_0}{1+m_1G_r}P_1\exp\left[i\left\{m_1(x-ct)-\frac{m_1G_i}{1+m_1G_r}\right\}\right], \tag{3.10}$$

where A_0 is the wave amplitude,

$$P_1=\{m_1(U-c)-U'\}e^{-m_1z}\left[1+m_1\int_z^\infty\left\{\left(\frac{U_\infty-c}{U-c}\right)^2-1\right\}dz\right]$$
$$+m_1(U-c)e^{-m_1z}\left[\left(\frac{U_\infty-c}{U-c}\right)^2-1\right], \tag{3.11}$$

and G_r and G_i denote the quantities given by

$$\int_0^\infty \left\{ \left(\frac{U_\infty - c}{U - c} \right)^2 - 1 \right\} dz = G_r + iG_i \,. \tag{3.12}$$

We compare Eqs. (3.10) and (3.11) with our results of measurements in the case of wind waves only. Using the wind profiles shown in Fig. 8 as well as $c \fallingdotseq 60$ cm/sec, we obtain

$$U - c \fallingdotseq 350 \text{ cm/sec}, \quad U' \fallingdotseq 22 \text{ sec}^{-1} \quad \text{and} \quad \int_z^\infty \{\quad\} dz \fallingdotseq 16.7$$

for $z = 3$ cm

and

$$U - c \fallingdotseq 400 \text{ cm/sec}, \quad U' \fallingdotseq 12 \text{ sec}^{-1} \quad \text{and} \quad \int_z^\infty \{\quad\} dz \fallingdotseq 12.2$$

for $z = 6$ cm.

Putting these values into Eq. (3.11) together with $m_1 \fallingdotseq 0.25$, we find that P_1 is definitely positive: $P_1 = 232$ for $z = 3$ cm and $P_1 = 105$ for $z = 6$ cm. If we assume the log-profile (3.1) with the values $z_0 \fallingdotseq 0.01$, $z_0 \fallingdotseq 0.03$ and $u_* \fallingdotseq 30$, then we obtain $G_i \fallingdotseq 0.34 \times \pi$. Though we cannot calculate the value of G_r, $(1 + m_1 G_r)$ can be assumed to be nearly the order of unity (cf. Phillips 1966, p. 101). If we take $1 + m_1 G_r \fallingdotseq 1.0$, then we obtain

$$\frac{m_1 G_i}{1 + m_1 G_r} \fallingdotseq 0.085 \times \pi \,.$$

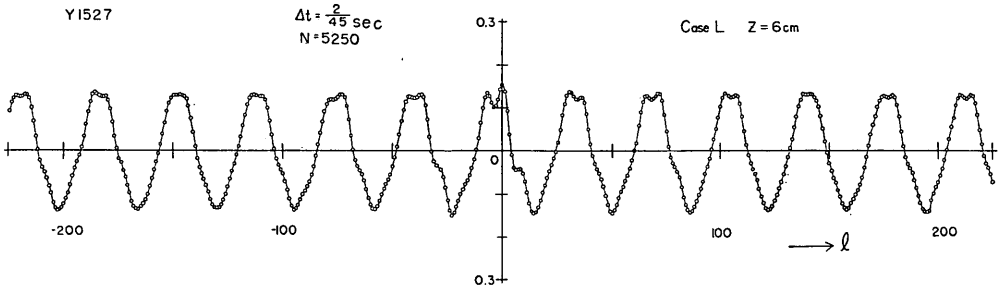

Fig. 23 Cross-Correlogram (superposed long waves, $z = 6$ cm)

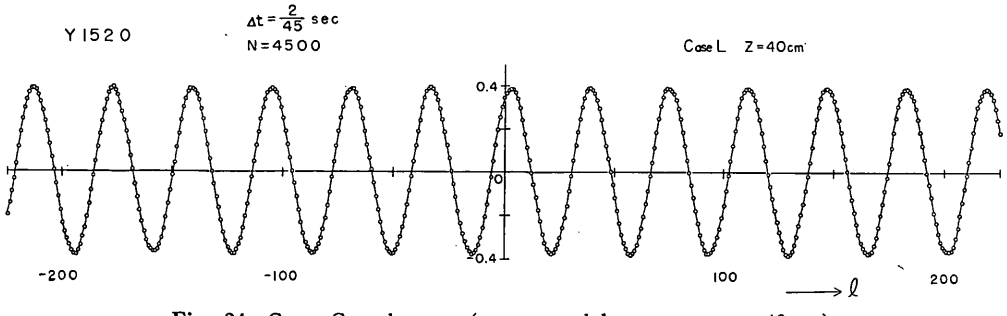

Fig. 24 Cross-Correlogram (superposed long waves, $z = 40$ cm)

Anyway the value of $m_1G_i/(1+m_1G_r)$ will be fairly small. Therefore it is found that the phase of u_1 given by (3.10) leads that of the wave, $\eta=A_0e^{im_1(x-ct)}$, by a small quantity $m_1G_i/(1+m_1G_r)$. This is very consistent with our experimental results.

Next we proceed to the results in case L (superposed long waves). The cross-correlograms at $z=6$ cm and 40 cm are shown in Figs. 23 and 24, and the cross-spectra at $z=6$ cm, 15 cm and 40 cm are shown in Figs. 25, 26 and 27, respectively. In this case the original long wave with a single period of 1.60 sec is so overwhelming that the wave spectrum takes the forms of a line spectrum. Similarly co- and quad-spectrum have a strongly concentrated peak at $f=0.625$ c/s. For the height of $z=6$ cm they also show some amount of density at the frequencies between 2 and 3 c/s corresponding to wind waves, but for $z=40$ cm they have no density except at $f=0.625$ c/s. The coherence at $z=6$ cm has the unexpectedly small value of 0.44 at $z=$ 0.625 c/s (in another run the value was only about 0.3), while it has considerable values up to 0.56 near $f=2.5$ c/s. This

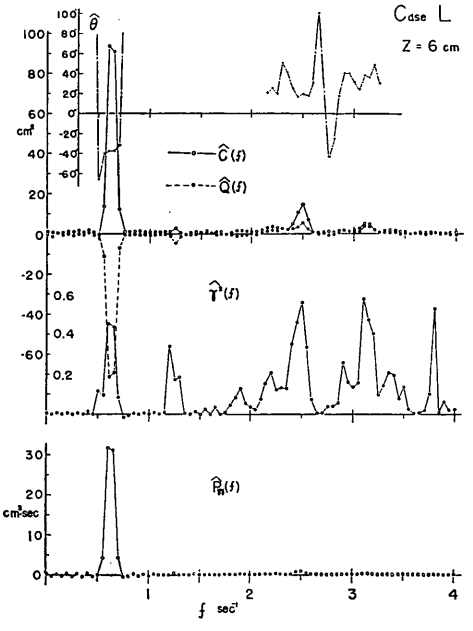

Fig. 25 Cross-Spectrum (superposed long waves, $z=6$ cm)

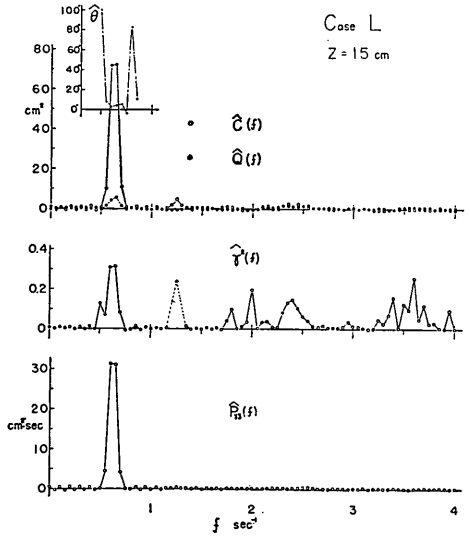

Fig. 26 Cross-Spectrum (superposed long waves, $z=15$ cm)

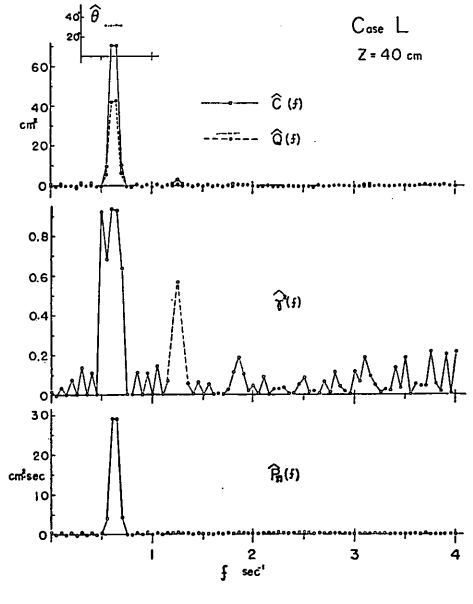

Fig. 27 Cross-Spectrum (superposed long waves, $z=40$ cm)

effect of wind waves on the coherence becomes nearly negligible at $z=15$ cm and completely disappears at $z=40$ cm. The coherence at $z=40$ cm has the values larger than 0.90 only near $f=0.625$ c/s. This variation of the coherence with height supports the conjection stated in § 3.2 concerning the behaviour of spectra at $f=0.625$ c/s in case L.

Here we use $\hat{\theta}_L$ to denote the value of phase lag at $f=0.625$ c/s (practically the average of those at $f=0.6$ and 0.65 c/s). At $z=40$ cm we find $\hat{\theta}_L=31°$. Eq. (3.7) suggests that this value is the very accurate estimate of the true phase lag since the coherence is very large there. In fact, the value $\hat{\theta}_L=43°$, obtained in another run where the wave gauge was placed 10.5 cm downwind of the hot-wire, is just equivalent to $\hat{\theta}_L \to 31°$ provided that we compensate it with the wave velocity $c \fallingdotseq 193$ cm/sec. However, the values $\hat{\theta}_L=-38°$ for $z=6$ cm and $\hat{\theta}_L=4°$ for $z=15$ cm, which are obtained from Figs. 25 and 26, respectively, seem to involve considerable uncertainty. We have also obtained the following (compensated) values in other runs with the above-mentioned distance of 10.5 cm and 0.4 cm: $\hat{\theta}_L=-25°$ and $-5°$ for $z=6$ cm; $\hat{\theta}_L=22°$ and $-1°$ for $z=15$ cm. Anyway it is very likely that $\hat{\theta}_L$ at $z=6$ cm take a small negative value. This is somewhat in contrast to the case of wind waves only. The height of $z=6$ cm in case L, where the mean wave height $H \fallingdotseq 5.6$ cm, is nearly comparable with the height of $z=3$ cm in case W with $H_{1/3} \fallingdotseq 2.6$ cm in the relative height; actually the each height is nearly the minimum height for measurements above the wave crests in each case. Nevertheless the degree of the wave-induced velocity fluctuations is found to be considerably higher at $z=3$ cm in case W than at $z=6$ cm in case L. A cause of this may be due to the difference of the wave steepness δ between case W $\left(\delta \fallingdotseq \frac{1}{10}\right)$ and case L $\left(\delta \fallingdotseq \frac{1}{50}\right)$.

Shemedin and Hsu (1966) measured the instantaneous velocity profiles above the crest and trough of a mechanically-generated wave from the simultaneous time records of the dynamic pressure of the pitot static tube fixed in space and the corresponding waves. Their results reveal that there is a definite difference between the velocity profile over the crest and trough, and further that the velocity at the same point fixed in space near the crest is larger over the crest than over the trough. Although we tried the same thing by using the hot-wire instead of the pitot tube in our case L, we could not detect such a difference successfully because there were much random fluctuations. However, the obtained results of the cross-correlation (or cross-spectrum) in case L indicate the nearly same thing. Though the coherence is not very large, an obvious correlation exists between the surface displacement η and the velocity fluctuation u' at $z=6$ cm and the convariance is positive (cf. Fig. 23):

$$(\overline{u'\eta})_{\tau=0}>0\,. \tag{3.13}$$

This indicates that the positive u' is statistically more related to the positive η and the negative u' to the negative η; the velocity averaged over the wave crest is larger than that averaged over the trough.

The rough order of magnitude of the velocity difference between over the crest and the trough may be found as follows. Neglecting the phase lag, we put

$$u'=b_1\cos\omega_1 t+u_1', \tag{3.14}$$

$$\eta=a_1\cos\omega_1 t+\eta_1, \tag{3.15}$$

where a_1 denotes the half of mean wave height and b_1 the half velocity difference. u_1' is essentially random, but at $z=6$ cm it may be somewhat correlated with wind waves (which are nearly represented by η_1) superposed on the long periodic waves. Then

$$\overline{u'\eta}=a_1b_1\times\frac{1}{2}+b_1\overline{\eta_1\cos\omega_1 t}+a_1\overline{u_1'\cos\omega_1 t}+\overline{u_1'\eta_1}. \tag{3.16}$$

The second and the following terms on the right hand side must be smaller than the first term and we boldly negelct them;

$$\overline{u'\eta}\fallingdotseq\frac{1}{2}a_1b_1. \tag{3.17}$$

Since $\overline{u'\eta}$ and a_1 are given, we can find b_1 from Eq. (3.17). From the computation for $z=6$ cm in case L (corresponding to Figs. 23 and 25), $(\overline{u'\eta})_{\tau=0}=14.93$ cm^2/sec and $a_1\fallingdotseq2.8$ cm. Consequently, we obtained $b_1\fallingdotseq10.7$ cm/sec. In the same way we found $b_1\fallingdotseq9.1$ cm/sec for $z=15$ cm and $b_1\fallingdotseq6.2$ cm/sec for $z=40$ cm. This is a very rough estimation but it may give at least a rough order of magnitude of the mean wave-induced velocity, especially at $z=40$ cm where the coherence is very large.

4. Conclusions

Wind velocity fluctuations were measured over the two kinds of wave in a wind-wave tunnel by using a linearized hot-wire anemometer, and cross-spectra between wind and waves as well as wind velocity spectra with a wide frequency range were estimated by the digital methods. The main findings obtained are as follows:

1) Mean wind profiles measured over superposed long waves at the fetch of 18.75 m are definitely different from that over wind waves only.

2) The divided spectral computation employed to cover a wide frequency range were reasonably successful with the 'degrees of freedom' used.

3) Wind velocity spectra obtained show a range of frequencies where the spectral density varies with the frequency nearly to the $-5/3$ power, and this range is extended to the much lower frequencies than expected from Kolmogoroff's theory.

4) In the case of wind waves only, the wave-induced velocity fluctuations have a considerable intensity at the lowest height ($z=3$ cm) above the wave crests, the spectra there showing a dominant peak at the frequency of the waves. They decrease fairly rapidly with height, and become almost negligible at the height of 15 cm.

5) In the case of superposed long waves, the wave-induced fluctuations are only moderately strong even near the wave crests ($z=6$ cm), the corresponding spectrum having a very small peak at the frequency of the long waves. However, they do not decay very much with height and remain at $z=40$ cm as

a dominant component of the spectrum.

6) The wave-induced fluctuations are nearly in phase with waves. In the case of wind waves only, the phase lags θ of the waves relative to the fluctuations are nearly in the range from 15° to 30°. While in the case of superposed long waves, very possibly θ has a small negative value at $z=6$ cm, but it takes a definite value of 31° at $z=40$ cm.

Acknowledgements

The authors wish to express their appreciation to Dr. T. Hamada, Chief of Hydraulic Laboratory, for much helpful advice and to Mr. A. Shibayama, Senior Research Engineer, for his co-operation in the maintenance of the experimental facilities.

References

1) Akaike, H. (1962) On the design of lag window for the estimation of spectra. *Ann. Inst. Stat. Math.*, **14**, 1-21.
2) Barnett, T. P. & Wilkerson, J. C. (1967) On the generation of wind waves as inferred from airborne radar measurement of fetch limited spectra. *J. Mar. Res.*, **25**, 292-328.
3) Batchelor, G. K. (1953) *The Theory of Homogeneous Turbulence.* Cambridge Univ. Press.
4) Bendat, J. S. & Piersol, A. G. (1966) *Measurement and Analysis of Random Data.* John Wiley & Sons, Inc.
5) Blackman, R. B. and Tukey, J. W. (1958) *The measurement of power spectra.* Dover Publications, New York.
6) Clauser, F. H. (1956) The turbulent boundary layer. *Adv. in Appl. Mech.*, **4**, 1-51, Academic Press.
7) Collis, D. C. & Williams, M. J. (1959) Two-dimensional convection from heated wires at low Reynolds numbers. *J. Fluid Mech.*, **6**, 357-384.
8) Corrsin, S. and Kistler, A. L. (1954) Free-Stream Boundaries of Turbulent Flows. *Tech. Notes Nat. Adv. Comm. Aero., Wash.*, No. 3133. Also *Rep.* No. 1244 (1955).
9) Grant, H. L., Stewart, R. W. and Moilliet, A. (1962) Turbulence spectra from a tidal channel. *J. Fluid Mech.*, **12**, 241-268.
10) Hamada, T. (1968) On some properties of wind over water waves (*in Japanese*). *Rep. of Port and Harbour Res. Inst.*, Vol. 7, No. 4, 3-22.
11) Hinze, J. O. (1959) *Turbulence.* McGraw-Hill Book Co.
12) Jenkins, G. M. (1963) Cross-Spectral Analysis and the Estimation of Linear Open Loop Transfer Functions. *Time Series Analysis*, John Wiley & Sons, Inc., 267-276.
13) Lighthill, M. J. (1962) Physical interpretation of the mathematical theory of wave generation by wind. *J. Fluid Mech.*, **14**, 385-394.
14) Lumley, J. L. & Panofsky, H. A. (1964) *The Structure of Atmospheric Turbulence.* John Wiley & Sons Inc., 239pp.
15) Miles, J. W. (1957) On the generation of surface waves by shear flows. *J. Fluid Mech.*, **3**, 185-204.
16) Miles, J. W. (1967) On the generation of surface waves by shear flows. Part 5. *J. Fluid Mech.*, **30**, 163-175.
17) Mitsuyasu, H. (1966) Interactions between Water Waves and Winds (I)—co-existent system of wind wave and regular oscillatory wave— *Rep. Res. Inst. for Appl. Mech. Kyushu Univ.* Vol. XIV, No. 48, 64-89.
18) Phillips, O. M. (1966) *The Dynamics of the Upper Ocean.* Cambridge Univ. Press., 261pp.

19) Pond, S., Stewart, R. W. & Burling, R. W. (1963) Turbulence spectra in the wind over waves. *J. Atmos. Sci.*, **20**, 319-324.
20) Pond, S., Smith, S. D., Hamblin, D. F. & Burling, R. W. (1966) Spectra of velocity and temperature fluctuations in the atmospheric boundary layer over the sea. *J. Atmos. Sci.*, **23**, 376-386.
21) Reichlen, F. (1967) Some turbulence measurements in water. *J. Eng. Mech. Div., ASCE*, Vol. 93, No. EM 2, 73-97.
22) Shemdin, O. H. & Hsu, E. Y. (1966) The Dynamics of Wind in the Vicinity of Progressive Water Waves. *Tech. Rep.* No. 66, *Dept. Civil Eng. Stanford Univ.*
22) Shemdin, O. H. & Hsu, E. Y. (1967) Direct measurement of aerodynamic pressure above a simple progressive gravity wave. *J. Fluid Mech.*, **30**, 403-416.
23) Smith, S. D. (1967) Thrust anemometer measurements of wind-velocity spectra and of Reynolds stress over a coastal inlet. *J. Mar. Res.*, **25**, 239-262.
24) Snyder, R. L. & Cox, C. S. (1966) A field study of the wind generation of ocean waves. *J. Mar. Res.*, **24**, 141-178.
25) Weiler, H. S. & Burling, R. W. (1967) Direct measurements of stress and spectra of turbulence in the boundary layer over the sea. *J. Atmos. Sci.*, **24**, 653-664.